

Turbulent mixing, restratification, and phytoplankton growth at a submesoscale eddy

J. R. Taylor¹

J.R. Taylor, Department of Applied Mathematics and Theoretical Physics, University of Cambridge, Wilberforce Road, CB3 0WA, UK, (J.R.Taylor@damtp.cam.ac.uk)

¹Department of Applied Mathematics and
Theoretical Physics, University of
Cambridge, Cambridge, UK

High resolution large-eddy simulations are used to study the influence of submesoscale mixed layer instability and small-scale turbulence on phytoplankton growth in light-limited conditions. Four simulations are considered with small-scale turbulence driven by varying levels of surface cooling. Significant small-scale turbulence is seen even without surface forcing, and the downward mixing of phytoplankton is sufficient to briefly delay the developing bloom. Moderate and strong values of the constant surface heat flux ($Q = -10, -100\text{W/m}^2$) are sufficient to prevent a bloom. In contrast to the critical depth hypothesis, the growth rate for phytoplankton does not appear to be controlled by the mixed layer depth. Instead, a comparison between the turbulent diffusivity above the compensation depth and a critical value predicted by the critical turbulence hypothesis closely matches the timing and magnitude of phytoplankton growth.

1. Introduction

Small free-floating algae known as phytoplankton account for nearly half of the global primary production and form the foundation of the marine food web [Longhurst *et al.*, 1995]. At high latitudes, a strong seasonal cycle in phytoplankton growth and concentration reflects changes in solar insolation, nutrient availability, water temperature, atmospheric forcing, and grazing pressure. A particularly striking feature of the annual cycle in phytoplankton concentration is a rapid growth event known as the spring bloom. Recently, renewed attention has been paid to the physical and biological factors that combine to allow net phytoplankton growth at the onset of the spring bloom (see, e.g. the recent reviews by Behrenfeld and Boss [2014]; Sathyendranath *et al.* [2015] and the references cited therein). This paper will focus on the physical factors that combine to permit phytoplankton growth and bloom initiation.

Two distinct but related mechanisms have been invoked to explain the influence of physical processes on the onset of phytoplankton blooms. The critical depth hypothesis originating in work by Gran and Braarud [1935], Riley [1946], and Sverdrup [1953] asserts that the depth of turbulent mixing of phytoplankton controls bloom timing. The depth of mixing is often associated with the mixed layer depth, although the active mixing layer does not necessarily coincide with a distinct mixed layer (e.g. Brainerd and Gregg [1995]). If they don't coincide, it might be more appropriate to use the mixing layer depth rather than the mixed layer depth in the critical depth hypothesis (e.g. Franks [2014] and Enriquez and Taylor [2015].) Critical turbulence theory, developed by Huisman *et al.* [1999] and Ebert *et al.* [2001], extends the critical depth hypothesis by allowing the strength of

turbulent mixing to vary. *Huisman et al.* [1999] predicted that phytoplankton blooms can occur when the turbulent diffusivity drops below a critical threshold, irrespective of mixed layer depth. *Taylor and Ferrari* [2011a] used this framework to link the level of turbulent mixing to convective forcing associated with wintertime surface cooling and proposed that in a homogeneous water column, blooms can develop as soon as the cooling ends - possibly before significant shoaling of the mixed layer and the development of stable density stratification.

When the hydrographic properties of the ocean vary laterally – specifically when there is a significant horizontal density gradient – the level of turbulence in the upper ocean is not entirely dependent on the level of forcing from the atmosphere and the mixed layer depth, but is also influenced by lateral exchange processes. Regions with strong horizontal density gradients, or fronts, are often associated with an along-front ‘thermal wind’ which balances the hydrostatic pressure gradient associated with the change in density. However, the thermal wind equilibrium is unstable to several distinct instabilities. Although their dynamics vary, these instabilities have the net effect of causing the front to slump, thereby increasing the vertical density gradient - a process known as restratification. This paper will focus on a particular instability termed ‘mixed layer instability’ or MLI, an ageostrophic baroclinic instability that is thought to be important in generating 1-10km submesoscale eddies in the upper ocean (e.g. *Boccaletti et al.* [2007]; *Fox-Kemper et al.* [2008]; *Thomas et al.* [2008]). Submesoscales are characterized by relatively large Rossby numbers, ($U/(fL) \sim 1$) where U and L are characteristic velocity and length scales and f is the Coriolis parameter) [*Thomas et al.*, 2008]. Since the motion is less constrained

by the Earth’s rotation, submesoscales induce large vertical velocities [*Mahadevan and Tandon, 2006*]

Fox-Kemper et al. [2008] introduced a parameterization for restratification by MLI written in terms of an overturning streamfunction that acts to flatten tilting isopycnals. Using this parameterization, *Mahadevan et al.* [2010] and *Mahadevan et al.* [2012] defined a restratification ratio comparing the relative importance of eddy-driven restratification and mixing due to wind forcing or convection. Here, we will only consider convective forcing. If B_0 is the surface buoyancy flux, the restratification ratio is

$$R_{MLI} = \frac{B_0 f}{M^4 H^2}, \quad (1)$$

where f is the Coriolis parameter, H is the mixed layer depth, and M is the magnitude of the horizontal buoyancy gradient. Note that *Mahadevan et al.* [2010] and *Mahadevan et al.* [2012] also included a scaling coefficient, $c_e = 0.06$, in the denominator of R_{MLI} . This coefficient is excluded here for simplicity, and all values given below use the form in Eq. (1).

Restratification by MLI can influence phytoplankton growth in two ways - by decreasing the mixed layer depth and hence the depth of mixing [*Mahadevan et al., 2012*], and by reducing the intensity of turbulent mixing [*Taylor and Ferrari, 2011b*]. Using two-dimensional numerical simulations, *Taylor and Ferrari* [2011b] found that symmetric and baroclinic instability can restratify the upper ocean and suppress vertical mixing. The resulting phytoplankton blooms were interpreted in terms of the critical turbulence hypothesis. Based on observations from the North Atlantic Bloom 2008 experiment and complementary numerical simulations, *Mahadevan et al.* [2012] observed restratification of

the mixed layer before the cessation of wintertime cooling, which the authors attributed to MLI. An increase in the vertically-averaged chlorophyll concentration appeared to coincide with the development of stable stratification, and preceded the end of winter convection by some 20 days. The authors interpreted the bloom using the critical depth hypothesis with a shoaling of the mixed layer driven by the development of MLI and submesoscale eddies.

The horizontal resolution of the model used in *Mahadevan et al.* [2012] was 1 km. Although their model permitted the development of submesoscale eddies, it was too coarse to resolve turbulent motions in the mixed layer. While the simulations of *Taylor and Ferrari* [2011b] had a much higher resolution ($\sim 10m$), they were two-dimensional, preventing them from capturing the rollup of submesoscale eddies and the interaction between small scale turbulence and mature baroclinic instability. This leaves important open questions: How is small-scale turbulent mixing influenced by the development of submesoscale eddies through MLI and how do phytoplankton respond to submesoscale and fine-scale turbulence in light-limited conditions?

Here, high resolution three-dimensional large-eddy simulations (LES) are used to examine the competition between turbulent mixing and restratification by MLI, and the implications for the onset of the spring bloom. The focus will be on the early stages of development of a submesoscale eddy and phytoplankton bloom, with simulations each running for several days of model time. Small-scale turbulence is forced by applying a uniform surface heat flux. The simulation setup is highly idealized and relatively small values are chosen for the mixed layer depth and the characteristic size of submesoscale

eddies to make the computations more tractable. The simulations are best thought of as numerical experiments rather than an attempt to replicate given ocean conditions. The convective forcing in particular is a useful way to generate small-scale turbulence, although in practice many other factors also contribute to upper ocean turbulence [Thorpe, 2005].

A key distinguishing feature of LES is that the largest turbulent motions are explicitly resolved. Therefore the competition between restratification and mixing by the largest turbulent motions is resolved rather than parameterized. As will be shown below, this distinction has significant implications for the extent and timing of restratification and phytoplankton growth in the simulation. In particular, the net growth of phytoplankton in the LES closely follows the strength of turbulent mixing and does not appear to be set solely by the mixed layer depth. This suggests that in addition to shoaling the mixed layer as argued by Mahadevan *et al.* [2012], submesoscales can influence the timing of the spring bloom by modifying the rate of turbulent mixing, consistent with the critical turbulence hypothesis.

2. Simulation Setup

A series of simulations of convectively-forced MLI are used to test the competition between turbulent mixing and submesoscale eddy-driven restratification. Although the simulations are highly idealized, they capture important physical processes that influence phytoplankton growth, specifically MLI and convective turbulence. The domain size is 1 km in each horizontal direction and 120 m in the vertical. This domain is resolved with 512 gridpoints in each horizontal direction and 64 gridpoints in the vertical. The grid is stretched in the vertical with higher resolution at the upper surface, with a grid spacing

ranging from 1.3 to 2.9m with the highest resolution at the surface. Further details of the numerical method are given in Appendix A.

Periodic boundary conditions are applied in both horizontal directions, and a background buoyancy gradient, $M^2 \equiv |\nabla b|$, is added to the governing equations to represent the influence of a large scale density gradient. Here, we match the background buoyancy gradient in *Mahadevan et al.* [2012] with the choice of $M^2 = 3 \times 10^{-8} \text{s}^{-2}$. The buoyancy field is initialized with a weakly stratified ‘mixed layer’ from $-60\text{m} < z < 0$, overlying a more strongly stratified thermocline. The buoyancy frequency, $N \equiv (\partial b / \partial z)^{1/2}$, is initially uniform in each layer and can be characterized using the ‘balanced Richardson number’ $Ri_B \equiv N^2 f^2 / M^4$ where f is the Coriolis parameter. In this case, the initial conditions prescribe $Ri_B = 1$ in the mixed layer and $Ri_B = 20$ in the thermocline. The weak stratification in the mixed layer ensures that the flow is not unstable to symmetric instability from the start of the simulation. The initial density at the mixed layer base is about $6 \times 10^{-4} \text{ kg/m}^3$ larger than the value directly above at the surface. This density difference is much smaller than typical thresholds used to define the mixed layer depth, justifying the term ‘mixed’ layer. Based on the initial mixed layer depth ($H = 60\text{m}$) and frontal strength ($M^2 = 3 \times 10^{-8} \text{s}^{-2}$), the fastest growing mode of MLI is expected to have a horizontal scale close to 1km [*Fox-Kemper et al.*, 2008]. The horizontal domain is therefore large enough to encompass the most unstable mode of MLI. The domain is not large enough to capture mesoscales or the interactions between multiple submesoscale eddies.

The simulations are forced by applying a destabilizing buoyancy flux at $z = 0$, equivalent to cooling the surface. Values of the surface heat flux and R_{MLI} defined in Eq. (1) are listed in Table 1. *Mahadevan et al.* [2012] found that phytoplankton blooms occur when $R_{MLI} \leq 0.06$. Therefore, the values of R_{MLI} considered here span an order of magnitude above and below the threshold predicted by *Mahadevan et al.* [2012]. Note that while *Mahadevan et al.* [2012] find that $R_{MLI} \simeq 0.06$ for a surface heat flux of $Q \simeq -100\text{W/m}^2$ and the same horizontal buoyancy gradient, our case with $R_{MLI} = 0.06$ corresponds to $Q \simeq -10\text{W/m}^2$. This difference is due to the shallower mixed layer depth used here ($H \simeq 60\text{m}$ here, compared with $H \simeq 300\text{ m}$ in *Mahadevan et al.* [2012]).

The phytoplankton concentration is modeled using the same equation as in *Taylor and Ferrari* [2011a, b]:

$$\frac{\partial P}{\partial t} + \mathbf{u} \cdot \nabla P = (\mu_0 e^{z/h_l} - m) P + \nabla \cdot ((\kappa + \kappa_{SGS}) \nabla P), \quad (2)$$

where \mathbf{u} is the resolved LES velocity field, μ_0 is the maximum growth rate, h_l is an e -folding depth, m is the mortality (loss) rate, and κ and κ_{SGS} are the constant molecular and subgrid-scale diffusivities, respectively. The parameters in Eq. (2) match those in *Taylor and Ferrari* [2011a]. Specifically, the maximum growth rate is $\mu_0 = 1\text{ day}^{-1}$, the loss rate is $m = 0.1\text{ day}^{-1}$, and $h_l = 5\text{ m}$. While Eq. (2) is highly idealized and neglects various factors including nutrient limitation, grazing, self-shading, cell sinking/buoyancy and motility, it provides a framework to study the influence of turbulence and eddy-driven restratification on phytoplankton growth under light-limited conditions. The phytoplankton model is initialized with a constant value $P = P_0$ in the mixed layer, with $P = 0$ below that

depth. Since Eq. (2) is linear in P , the results will be independent of P_0 . The simulation parameters are summarized in Table 1.

3. Results

Figure 1 shows visualizations of the buoyancy field at $t = 3$ days for the simulations with no surface cooling ($Q = 0$) and moderate forcing ($Q = -10 \text{ W/m}^2$). In both cases MLI has fully developed by this time and has led to a single coherent submesoscale eddy with a horizontal scale close to the domain size $L \simeq 1 \text{ km}$, consistent with the most unstable mode associated with MLI. Unlike some previous studies (e.g. *Mahadevan and Tandon* [2006]; *Mahadevan et al.* [2012]; *Fox-Kemper et al.* [2008]; *Capet et al.* [2008]), the resolution used here is sufficient to capture the largest three-dimensional turbulent overturns. In the case with $Q = 0$, small-scale turbulence is visible along the fronts that form at the edge of the submesoscale eddy which is also reflected in enhanced vertical velocity (see Appendix A). Since this simulation is not forced by wind or convection and the flow is initially stable to Kelvin-Helmholtz and symmetric instabilities, the small-scale turbulence that arises is due to a down-scale energy transfer from the submesoscale. As described below, strong vertical motions in this simulation briefly delay the phytoplankton bloom, despite the lack of surface forcing. Surface cooling provides another source of small-scale turbulence. In the simulation with $Q = -10 \text{ W/m}^2$, small convective plumes are visible superimposed on a submesoscale eddy (Fig. 1, right panel).

The competition between restratification by MLI and mixing by small-scale turbulence can be assessed by examining the horizontally-averaged stratification. In all cases the mean stratification reaches a nearly steady state after about 2 days. Figure 2(a) shows

profiles of the balanced Richardson number, $Ri_B = \overline{N^2} f^2 / M^4$, where $\bar{\cdot}$ denotes an average over both horizontal directions. Note that here the vertical coordinate is defined to be increasing upwards such that $z < 0$. For reference, the initial Ri_B profile is indicated with a dashed line. With the exception of a thin surface layer, the stratification increases relative to the initial state when $Q \geq -10 \text{ W/m}^2$. Significant deepening of the mixed layer is evident in the case with $Q = -100 \text{ W/m}^2$, although a weak stable stratification persists in the region between $-70\text{m} < z < -20\text{m}$.

Vertical profiles of the horizontal mean phytoplankton concentration are shown in Figure 2(b). For reference, the initial phytoplankton profile is shown using a dashed line. Only the case with $Q = -100 \text{ W/m}^2$ has a uniform mean phytoplankton profile above the critical depth ($H_c = 50\text{m}$). All other cases show varying degrees of surface intensification, reflecting the net growth rate, $\mu(z) - m$, shown in Figure 2(c). Significant spatial variability also develops in the phytoplankton concentration, particularly when the surface heat flux is weak. In the case with $Q = 0$, the phytoplankton concentration at $t = 3$ days varies by more than a factor of 5 at $z = -10\text{m}$ (see Appendix A).

Timeseries of the surface phytoplankton concentration (Figure 3a) show very different behavior amongst the simulations. Without forcing ($Q = 0$, blue line), phytoplankton grow at the surface for the first 1.5 days, and the surface concentration then decreases briefly before resuming its growth. Very weak convective forcing ($Q = -1 \text{ W/m}^2$, cyan line) is enough to significantly reduce the increase in the surface phytoplankton concentration. In contrast, aside from a brief spinup period, the surface concentration decreases

monotonically when $Q = -10$ and -100 W/m^2 . Depth-time plots of the horizontally-averaged stratification and phytoplankton concentration can be found in Appendix A.

If phytoplankton remained at the surface and grew unchecked with the net growth rate (0.9 days^{-1}), their concentration would increase by more than a factor of 90 in a 5 day period. In all simulations here, the surface phytoplankton concentration is much less than the maximum possible growth. Since the phytoplankton model (Eq. 2) has a constant net growth rate, limitation of the surface phytoplankton growth must occur through downward advection or diffusion.

The time evolution of the integrated phytoplankton biomass can be calculated by integrating Eq. (2) over the full model domain. Due to the use of periodic boundary conditions in the horizontal directions and a no flux boundary condition at the top boundary, the integrated phytoplankton biomass satisfies a simple equation

$$\frac{\partial}{\partial t} \int_V P dV = L_x L_y \int_{-L_z}^0 (\mu_0 e^{z/h_l} - m) \bar{P} dz, \quad (3)$$

where L_x , L_y , and L_z are the dimensions of the full computational domain, and \bar{P} is the horizontal mean phytoplankton concentration. The growth of integrated biomass depends only on the vertical structure of \bar{P} . Timeseries of the integrated phytoplankton biomass, $\int P dV$, are shown in Figure 3(a). In the cases with $Q = -10 \text{ W/m}^2$ and $Q = -100 \text{ W/m}^2$, $\int P dV$ decreases monotonically. When $Q = -1 \text{ W/m}^2$, $\int P dV$ remains nearly constant, while only the case without forcing ($Q = 0$) exhibits strong growth.

It is clear from Figure 2(a) that the weakly stratified ‘mixed layer’ deepens in the simulation with strongest forcing ($Q = -100 \text{ W/m}^2$). However, it isn’t clear precisely how to define the time-dependent mixed layer depth, particularly when a stable stratification

develops at the surface. *Mahadevan et al.* [2012] defined the mixed layer depth as the location where the potential density is 0.01 kg/m^3 larger than at the surface. With this definition, the mixed layer base is deeper than 100m and well below the critical depth in all cases. A much more sensitive threshold of $\Delta\rho = 6 \times 10^{-4} \text{ kg/m}^3$ tuned to match the initial density change in the upper 60m does yield shoaling of the mixed layer when $Q = 0, -1,$ and -10 W/m^2 , but the mixed layer depth is very similar in these three cases (the mixed layer depth evolution using both definitions is shown in Figure 7 in Appendix A.) The ambiguity in the definition of mixed layer depth is one of the inherent difficulties in applying the critical depth hypothesis to periods of restratification, particularly when the degree of restratification varies with depth.

Figure 3(c) shows a time series for another choice of the mixed layer depth, defined as the shallowest depth where $N^2 < 5 \times 10^{-7} \text{ s}^{-2}$. This value was chosen because it captures the transition from the weakly stratified surface layer to the thermocline in all cases, although as noted above, this is not a unique definition. Defined in this way, the mixed layer base remains below the critical depth in all simulations for all times, which is also the case using the definition in *Mahadevan et al.* [2012]. Notably, the mixed layer depth is nearly identical in the cases with $Q=0, -1,$ and -10 W/m^2 , while the mixed layer deepens monotonically when $Q = -100 \text{ W/m}^2$.

Two perhaps unexpected results have emerged thus far. First, in the unforced simulation ($Q = 0$), the surface phytoplankton concentration decreases between about 1.5 and 2.5 days, and growth in integrated phytoplankton biomass virtually stops, before the bloom resumes. Second, the mixed layer depth and stratification profiles are very similar in

the cases with $Q = 0, -1,$ and -10 W/m^2 , but the phytoplankton response in these three simulations is fundamentally different with a surface-intensified bloom when $Q = 0$ and decay when $Q = -10 \text{ W/m}^2$. Both results can be explained by invoking the critical turbulence hypothesis and examining the intensity of turbulent mixing.

Taylor and Ferrari [2011a] used a simple model to interpret bloom onset via the critical turbulence hypothesis by comparing characteristic timescales associated with net phytoplankton growth and mixing in two layers separated by the compensation depth, h_c , where the local growth rate exactly balances the local loss rate. Using this model, they derived an approximation to the critical turbulent diffusivity,

$$\kappa_c \simeq h_c^2 \frac{\mu_{eff}^2}{m_{eff}}, \quad (4)$$

where μ_{eff} is a representative growth rate above the compensation depth, and m_{eff} is a representative net loss rate below the compensation depth. Note that μ_{eff} and m_{eff} are both constant in this expression. The critical turbulence hypothesis then predicts net phytoplankton growth when the turbulent diffusivity, κ_T , is less than the critical κ_c .

The turbulent diffusivity can be directly diagnosed from the phytoplankton budget in the simulations presented here. However, the turbulent diffusivity varies in space and time, making a comparison with κ_c more difficult. Nevertheless, we can construct a representative turbulent diffusivity to compare with κ_c by averaging the vertical flux and the vertical gradient of phytoplankton over the three-dimensional volume above the compensation depth, i.e.

$$\kappa_T \equiv -\frac{\langle wP \rangle}{\langle \partial P / \partial z \rangle}, \quad (5)$$

where angled brackets denote an average over all points above the compensation depth ($z > h_c$). When defined pointwise rather than using a volume average, κ_T is very noisy and can become large in magnitude or negative, particularly where $\partial P/\partial z$ is small. The choice of the compensation depth as the lower bound of the volume window is motivated by the definition of the critical diffusivity in Eq. (4) which involves the net growth rate above the compensation depth. The average turbulent diffusivity defined in Eq. (5) is shown as a function of time in Figure 3(b). The critical turbulent diffusivity calculated from Eq. (4) is shown using a dashed line, where μ_{eff} is calculated by averaging $\mu(z) - m$ above the critical depth, and $m_{eff} = m$.

For the simulations reported here, the rate of change of integrated phytoplankton biomass, $\int P dV$, closely follows the turbulent diffusivity defined in Eq. (5). Generally, when $\kappa_T < \kappa_C$, the phytoplankton biomass increases, and the converse is also true. The magnitude of the growth and decay in phytoplankton biomass also closely corresponds to the magnitude of κ_T . These results are consistent with the critical depth hypothesis. The correspondence between κ_T and phytoplankton growth is remarkable considering that κ_T is calculated only from model data above the compensation depth (here $h_c \simeq 11$ m).

Submesoscale MLI appears to have two competing influences on the vertical flux of phytoplankton. Without forcing, subduction of phytoplankton associated with MLI is sufficient to temporarily decrease the surface phytoplankton concentration and delay the bloom. On the other hand, restratification suppresses vertical mixing and hence the vertical phytoplankton flux. The outcome of this competition can be quantified by comparing profiles of the turbulent diffusivity from the simulations discussed here with the simula-

tions from *Taylor and Ferrari* [2011a] with the same phytoplankton model but without MLI (see Figure 8). When $Q = -1$ and -10 W/m^2 , κ_T is reduced by about a factor of 5 in the simulations with MLI, indicating suppression of mixing by restratification. On the other hand, when $Q = -100 \text{ W/m}^2$, the profiles of κ_T are very similar identical in the upper 25m , suggesting that mixing by convection is relatively unaffected by MLI in this region.

4. Discussion

High resolution large-eddy simulations (LES) have been used to examine the competition between gravitational slumping of a front (restratification) driven by a submesoscale baroclinic instability and vertical mixing associated with convective forcing. The simulations used a relatively small domain (one square kilometer) that is nonetheless large enough to resolve the most unstable mode of mixed layer instability (MLI), while resolving the largest turbulent eddies with a horizontal grid spacing close to 2m . A fixed background horizontal density gradient supplies potential energy to MLI, and a series of simulations was conducted with different levels of surface cooling. A simplified phytoplankton model is used to examine the impact of this competition on phytoplankton growth under light limited conditions. In three of the simulations, with surface heat fluxes of $Q = 0, -1, -10\text{W/m}^2$, the stable density stratification increased above the critical depth, and yet only the unforced simulation ($Q = 0$) showed a significant bloom. Weak phytoplankton growth was seen in the simulation with $Q = -1\text{W/m}^2$, while the simulations with $Q = -10$ and -100 W/m^2 exhibited continual decline of the integrated phytoplankton concentration.

The results presented here are not consistent with the hypothesis of *Mahadevan et al.* [2012] that submesoscale eddies trigger phytoplankton blooms by shoaling the mixed layer above the critical depth. Rather, the LES results suggest that phytoplankton blooms can be delayed or suppressed by downward mixing of phytoplankton cells even when a stable stratification develops above the critical depth. The close correspondence between phytoplankton growth and decay, and the intensity of turbulent mixing diagnosed using a turbulent diffusivity (Fig. 3) suggests that the critical turbulence hypothesis can be used to describe the influence of submesoscales on phytoplankton growth.

There are several important differences between the LES model and the model used by *Mahadevan et al.* [2012] which might explain the difference in the results. The LES directly resolves the largest three-dimensional turbulent motions responsible for mixing phytoplankton in the upper ocean. In contrast, the model used by *Mahadevan et al.* [2012] used a grid spacing of 1km in the horizontal directions, and parameterized the vertical turbulent mixing. In their model, vertical mixing was parameterized as a prescribed function of depth which was explicitly linked to the mixed layer depth. The magnitude of the vertical mixing coefficient depended on the surface wind stress, but not on the local stratification or shear. Therefore, unlike the LES model used here, the model of *Mahadevan et al.* [2012] does not account for changes in turbulent mixing that might result from stratification within the mixed layer.

On the other hand, the LES model is highly idealized and misses important physical and biological processes. Notably, only convective forcing is considered here, but mixing driven by wind and Langmuir turbulence are likely to be a major factor in setting the intensity

of mixing in the upper ocean. Indeed, *Mahadevan et al.* [2012] reported that the vertical velocities observed from a Lagrangian float during the North Atlantic Bloom Experiment were closely correlated with the surface wind stress. The competition between turbulent mixing driven by wind, Langmuir circulation and restratification by submesoscales has been examined recently [*Hamlington et al.*, 2014; *Smith et al.*, 2015], although the influence of this competition on phytoplankton blooms remains an open question. The phytoplankton model used here also neglects many factors other than light limitation, including grazing pressure which might present another mechanism for triggering the spring phytoplankton bloom [*Behrenfeld*, 2010; *Boss and Behrenfeld*, 2010].

The sensitivity of vertical mixing to the presence of submesoscales presents a major challenge for future observational and modelling work. Turbulent mixing is much more difficult to measure than density stratification, but the results presented here suggest that the former is needed to accurately characterize phytoplankton growth during light limited conditions. In many ocean modelling applications, it is not feasible to resolve submesoscale dynamics, and the ability to resolve the three-dimensional turbulence responsible for vertical mixing in these cases is well out of reach. A parameterization for MLI was proposed by *Fox-Kemper et al.* [2008] and has already been implemented in several ocean models. The parameterization improves the ability of ocean models to capture the restratification induced by submesoscale eddies, yet does not explicitly modify the turbulent mixing scheme. Further work is needed to examine the direct influence of submesoscale processes on turbulent mixing.

Appendix A: Supplementary Online Material

A1. Numerical method

The numerical simulations use DIABLO, an open-source non-hydrostatic computational fluid dynamics code developed in *Taylor* [2008]. The code solves the incompressible Boussinesq equations using a combination of a pseudo-spectral method to calculate horizontal derivatives and second-order finite differences to calculate vertical derivatives. The time-stepping algorithm is a mixed implicit/explicit scheme using a 3rd order Runge Kutta method and Crank-Nicolson for viscous/diffusive terms. Further details about the numerical method are available in *Taylor* [2008].

An LES solves a low-pass filtered version of the governing equations. In order to close the equations, a subgrid-scale model is needed to represent the influence of unresolved velocity and density fluctuations on the resolved fields. Here, we have used a modified version of the constant Smagorinsky model proposed by *Kaltenbach et al.* [1994]. This model has been used previously in several previous related studies (e.g. *Taylor and Ferrari* [2010, 2011a]; *Thomas et al.* [2013]). For simplicity, the subgrid-scale diffusivity for density and phytoplankton are assumed to match the viscosity (the subgrid-scale Prandtl and Schmidt numbers are set to 1).

The model is run in a so-called ‘frontal zone’ configuration introduced by *Taylor and Ferrari* [2009]. In this configuration, the total buoyancy, b_T , is decomposed into a linear profile plus perturbations:

$$b_T(x, y, z, t) = M^2 x + b'(x, y, z, t). \quad (\text{A1})$$

This form is inserted into the governing equations to yield evolution equations for b' . The model then solves these equations with periodic boundary conditions applied to b' . Effectively, this keeps the difference in total buoyancy across the domain constant in space and time. Although this configuration is artificial, it represents intensification of buoyancy gradients due to frontogenesis or differential heating at scales that are too large to be resolved in the domain. To prevent spurious reflections of internal gravity waves from the bottom of the computational domain, a sponge layer was added from 120-140m.

Before starting convective forcing and initializing the phytoplankton model, MLI was allowed to develop from a small-amplitude random perturbation. To reduce the computational cost, this spinup was performed using a coarser resolution with 128 gridpoints in each horizontal direction, but the same vertical grid spacing. During the spinup period, the volume-averaged turbulent kinetic energy increases from $5.5 \times 10^{-12} \text{m}^2/\text{s}^2$ to $3.0 \times 10^{-8} \text{m}^2/\text{s}^2$, and the energy at the end of the spinup was dominated by the most unstable mode with a characteristic horizontal scale of 1km. Spectral interpolation is then used to initialize each of the high resolution simulations. For convenience, $t = 0$ corresponds to the end of the spinup period, when the phytoplankton model is initialized and convective forcing begins.

A2. Visualizations

Figure 4 shows 3D visualizations of the vertical velocity and phytoplankton concentration from the simulations with $Q = 0$ and $Q = -10 \text{W}/\text{m}^2$ at $t = 3.5$ days (the same time as shown in Figure 1). The vertical velocity is relatively large, exceeding 5 mm/s, in the unforced simulation ($Q = 0$). Large vertical velocity occurs in bands wrapped around

the submesoscale eddy and in intermittent bursts. The turbulent bursts are qualitatively similar to those seen in recent studies of stratified turbulence [*Rorai et al.*, 2014, e.g.]. When $Q = -10\text{W/m}^2$, the vertical velocity is up to three times larger, exceeding 1.5 cm/s. Here, strong downdrafts are visible along lines wrapped around the submesoscale eddy. It seems likely that this strong vertical velocity is associated with submesoscale frontogenesis [*Shakespeare and Taylor*, 2013, e.g.] driven by strain associated with the submesoscale eddy. Possible indications of horizontal shear instabilities are also visible along this band, notably on the right side of the image.

The corresponding phytoplankton concentration is shown in the bottom row of Figure 4. In the unforced case (Fig. 4 lower left panel) swirls of high phytoplankton concentration are seen wrapping in and around the submesoscale eddy. At a given horizontal level, the phytoplankton concentration varies by more than a factor of 5, indicating the very strong spatial inhomogeneity that develops. In contrast, the phytoplankton concentration is more uniform in the simulation with $Q = -10\text{W/m}^2$ (Fig. 4 lower right panel), and the maximum concentration is significantly lower. Still, physical features of the flow are visible in the phytoplankton concentration including the submesoscale eddy, small-scale convective motions, and banding in the vertical.

A3. Time evolution of vertical density and phytoplankton profiles

Figure 2(a) showed profiles of the bulk Richardson number, $Ri_B = \overline{N^2}f^2/M^4$ at 3.5 days of simulation time. A more complete picture of the mean stratification can be seen using depth-time plots of the balanced Richardson number as shown in Figure 5. Note that here the colorbar is saturated to emphasize the stratification that develops within

the mixed layer. In the three cases with the weakest forcing ($Q = 0, -1, \text{ and } -10 \text{ W/m}^2$), the boundary between the strongly stratified thermocline and the mixed layer remains relatively constant, consistent with the mixed layer depth shown in Figure 3(c). These cases all develop stronger stratification near the surface, although the strength of this stratification decreases with increasing forcing.

A non-zero stratification with $Ri_B \simeq 1$ develops in the case with $Q = -100 \text{ W/m}^2$, underlying a region with $N^2 < 0$ and active convection. This is consistent with the dynamics of forced symmetric instability (SI) reported in *Taylor and Ferrari* [2010] where a prediction for the boundary between the convective and SI layers is consistent with the results presented here. An important difference here is that mixed layer eddies have strongly distorted the fronts on which SI might be active. A detailed analysis of the interaction between forced SI and MLI will be left for future work.

A similar depth-time plot of the horizontally-averaged phytoplankton concentration is shown in Figure 6. Large near-surface concentrations quickly develop in the simulations with $Q = 0$ and -1 W/m^2 . The reduction in the surface phytoplankton concentration seen in Figure 3(a) from about 1.5-2 days in the case with $Q = 0$ is accompanied by an increase in the phytoplankton concentration between $-25\text{m} < z < 0$. This is consistent with the interpretation that downward advection of phytoplankton associated with strong frontogenesis is responsible for delaying the phytoplankton bloom in this case.

A4. Mixed layer depth

As discussed in the main text, the definition of mixed layer depth is somewhat ambiguous given the significant vertical structure in the upper ocean stratification seen here,

particular in the cases with weak convective forcing. In addition to the definition used in the main text, two other examples of the mixed layer depth are shown in Figure 7. For reference, the critical depth, $H_c = 50m$, is indicated using a thin dashed black line.

The definition used by *Mahadevan et al.* [2012] is the depth where the local potential density changes by 0.01 kg/m^3 from the surface value. This definition is shown using dashed lines in Figure 7. As noted in the text, the initial stratification in the mixed layer is very weak by traditional measures, with a change of $5.4 \times 10^{-4} \text{ kg/m}^3$ in the upper 60m at the start of each simulation. Therefore to reach a value of 0.01 kg/m^3 , this definition of the mixed layer must include some of the more strongly stratified thermocline. In fact, the initial mixed layer depth using this criteria is about 110m. The mixed layer, defined in this way, shoals very slightly in the simulations with weak convective forcing, but always remains larger than 100m, and much deeper than the critical depth of $H_c = 50m$.

A more sensitive definition of the mixed layer depth can be constructed using the initial density difference in the upper 60m. The mixed layer depth calculated using this definition is shown as dash-dotted lines in Figure 7. In the LES, a convective layer with $N^2 < 0$ develops near the surface. To avoid this convective layer as much as possible, a threshold of $6 \times 10^{-4} \text{ kg/m}^3$ is chosen using the difference between the local density and the density at a depth of 10m. With this definition, the restratification in the cases with $Q = 0, -1$, and -10 W/m^2 is sufficient to shoal the mixed layer above the critical depth at about 1.5 days of simulation time, while the mixed layer remains below the critical depth in the simulation with $Q = -100 \text{ W/m}^2$. Importantly, the mixed layer depth is very similar in the cases with $Q = 0, -1$, and -10 W/m^2 which have very similar density profiles but

very different phytoplankton responses. The timeseries of the mixed layer depth and critical depth and the surface and depth-integrated phytoplankton concentration shown in Figures 3(a) and (b), are not consistent with the critical depth hypothesis.

References

- Behrenfeld, M. (2010), Abandoning Sverdrup's Critical Depth Hypothesis on phytoplankton blooms, *Ecology*, *91*(4), 977–989.
- Behrenfeld, M. J., and E. S. Boss (2014), Resurrecting the ecological underpinnings of ocean plankton blooms, *Annual Review of Marine Science*, *6*, 167–194.
- Boccaletti, G., R. Ferrari, and B. Fox-Kemper (2007), Mixed layer instabilities and re-stratification, *Journal of Physical Oceanography*, *37*(9), 2228–2250.
- Boss, E., and M. Behrenfeld (2010), In situ evaluation of the initiation of the north atlantic phytoplankton bloom, *Geophysical Research Letters*, *37*(18), L18,603.
- Brainerd, K., and M. Gregg (1995), Surface mixed and mixing layer depths, *Deep-Sea Research I*, *42*(9), 1521–1543.
- Capet, X., J. C. McWilliams, M. J. Molemaker, and A. Shchepetkin (2008), Mesoscale to submesoscale transition in the california current system. part i: Flow structure, eddy flux, and observational tests, *Journal of Physical Oceanography*, *38*(1), 29–43.
- Ebert, U., M. Arrayas, N. Temme, B. Sommeijer, and J. Huisman (2001), Critical conditions for phytoplankton blooms, *Bulletin of Mathematical Biology*, *63*, 1095–1124.
- Enriquez, R. M., and J. R. Taylor (2015), Numerical simulations of the competition between wind-driven mixing and surface heating in triggering spring phytoplankton blooms, *ICES Journal of Marine Science: Journal du Conseil*, p. fsv071.
- Fox-Kemper, B., R. Ferrari, and R. Hallberg (2008), Parameterization of mixed layer eddies. part i: Theory and diagnosis, *Journal of Physical Oceanography*, *38*(6), 1145–1165.

- Franks, P. J. (2014), Has sverdrup's critical depth hypothesis been tested? mixed layers vs. turbulent layers, *ICES Journal of Marine Science: Journal du Conseil*, p. fsu175.
- Gran, H., and T. Braarud (1935), A quantitative study on the phytoplankton of the Bay of Fundy and the Gulf of Maine (including observations on hydrography, chemistry and morbidity), *Journal Biology Board Canada*, 1, 219–467.
- Hamlington, P. E., L. P. Van Roekel, B. Fox-Kemper, K. Julien, and G. P. Chini (2014), Langmuir–submesoscale interactions: Descriptive analysis of multiscale frontal spin-down simulations, *Journal of Physical Oceanography*, 44(9), 2249–2272.
- Huisman, J., P. van Oostveen, and F. Weissing (1999), Critical depth and critical turbulence: Two different mechanisms for the development of phytoplankton blooms, *Limnology and Oceanography*, 44(7), 1781–1787.
- Kaltenbach, H.-J., T. Gerz, and U. Schumann (1994), Large-eddy simulation of homogeneous turbulence and diffusion in stably stratified shear flow, *Journal of Fluid Mechanics*, 280, 1–40.
- Longhurst, A., S. Sathyendranath, T. Platt, and C. Caverhill (1995), An estimate of global primary production in the ocean from satellite radiometer data, *Journal of Plankton Research*, 17(6), 1245–1271.
- Mahadevan, A., and A. Tandon (2006), An analysis of mechanisms for submesoscale vertical motion at ocean fronts, *Ocean Modelling*, 14(3), 241–256.
- Mahadevan, A., A. Tandon, and R. Ferrari (2010), Rapid changes in mixed layer stratification driven by submesoscale instabilities and winds, *Journal of Geophysical Research: Oceans (1978–2012)*, 115(C3).

- Mahadevan, A., E. D'Asaro, C. Lee, and M. J. Perry (2012), Eddy-driven stratification initiates north atlantic spring phytoplankton blooms, *Science*, 337(6090), 54–58.
- Riley, G. (1946), Factors controlling phytoplankton populations on Georges Bank, *Journal of Marine Research*, 6, 54–72.
- Rorai, C., P. Mininni, and A. Pouquet (2014), Turbulence comes in bursts in stably stratified flows, *Physical Review E*, 89(4), 043,002.
- Sathyendranath, S., R. Ji, and H. I. Browman (2015), Revisiting sverdrup's critical depth hypothesis, *ICES Journal of Marine Science: Journal du Conseil*, 72(6), 1892–1896.
- Shakespeare, C. J., and J. Taylor (2013), A generalized mathematical model of geostrophic adjustment and frontogenesis: uniform potential vorticity, *Journal of Fluid Mechanics*, 736, 366–413.
- Smith, K. M., P. E. Hamlington, and B. Fox-Kemper (2015), Effects of submesoscale turbulence on ocean tracers, *Journal of Geophysical Research: Oceans*.
- Sverdrup, H. (1953), On conditions for the vernal blooming of phytoplankton, *Journal du Conseil International pour l'Exploration de la Mer*, 18, 287–295.
- Taylor, J. (2008), Numerical simulations of the stratified oceanic bottom boundary layer, Ph.D. thesis, University of California, San Diego.
- Taylor, J., and R. Ferrari (2010), Buoyancy and wind-driven convection at a mixed-layer density fronts, *Journal Physical Oceanography*, 40, 1222–1242.
- Taylor, J. R., and R. Ferrari (2009), On the equilibration of a symmetrically unstable front via a secondary shear instability, *Journal of Fluid Mechanics*, 622, 103–113.

Taylor, J. R., and R. Ferrari (2011a), Shutdown of turbulent convection as a new criterion for the onset of spring phytoplankton blooms, *Limnology and Oceanography*, 56(6), 2293–2307.

Taylor, J. R., and R. Ferrari (2011b), Ocean fronts trigger high latitude phytoplankton blooms, *Geophysical Research Letters*, 38(23).

Thomas, L. N., A. Tandon, and A. Mahadevan (2008), Submesoscale processes and dynamics, *Ocean Modeling in an Eddying Regime, Geophys. Monogr. Ser.*, 177, 17–38.

Thomas, L. N., J. R. Taylor, R. Ferrari, and T. M. Joyce (2013), Symmetric instability in the gulf stream, *Deep Sea Research Part II: Topical Studies in Oceanography*, 91, 96–110.

Thorpe, S. (2005), *The turbulent ocean*, Cambridge University Press, Cambridge.

Table 1. Simulation parameters

L_x, L_y, L_z	1000,1000,140 (m)
$\Delta x, \Delta y, \Delta z$	2,2,1.3-3 (m)
M^2	3×10^{-8} (s^{-2})
f	10^{-4} (s^{-1})
Q	0, -1, -10, -100 (W/m^2)
R_{MLI}	(0,0.006,0.06,0.6)
μ_0, m	1, 0.1 (day^{-1})
h_l	5 (m)

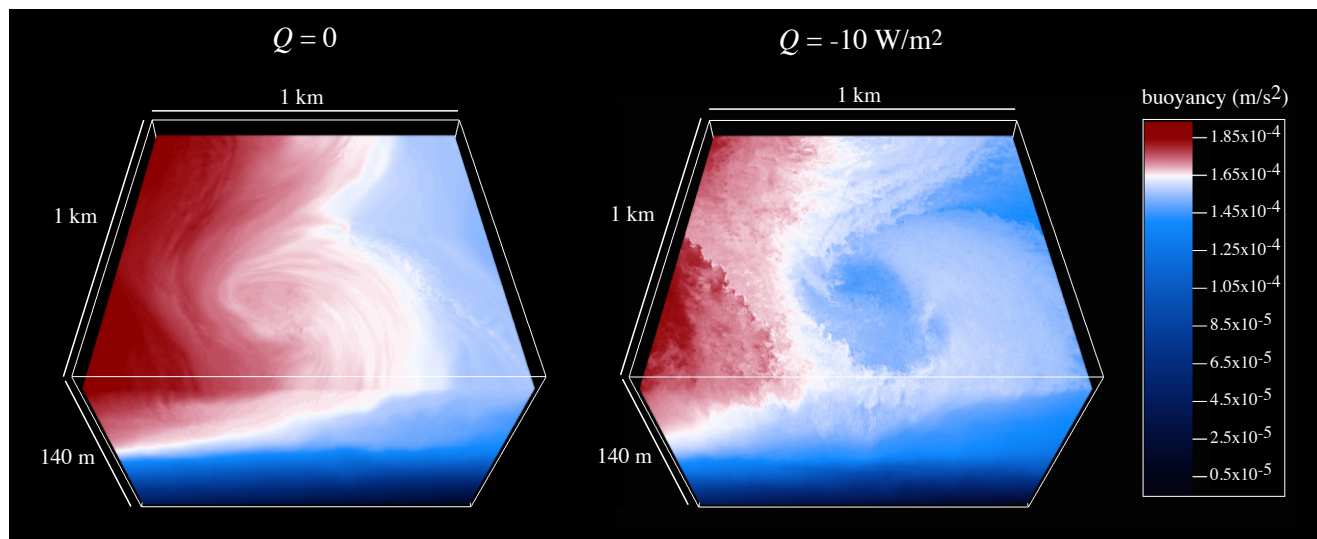


Figure 1. Visualizations of buoyancy at $t = 3.5$ days from simulations with surface heat fluxes of $Q = 0$ and $Q = -10W/m^2$. An arbitrary constant has been subtracted from the buoyancy such that the minimum value is zero. The upper slice shows the buoyancy at a depth of 10m.

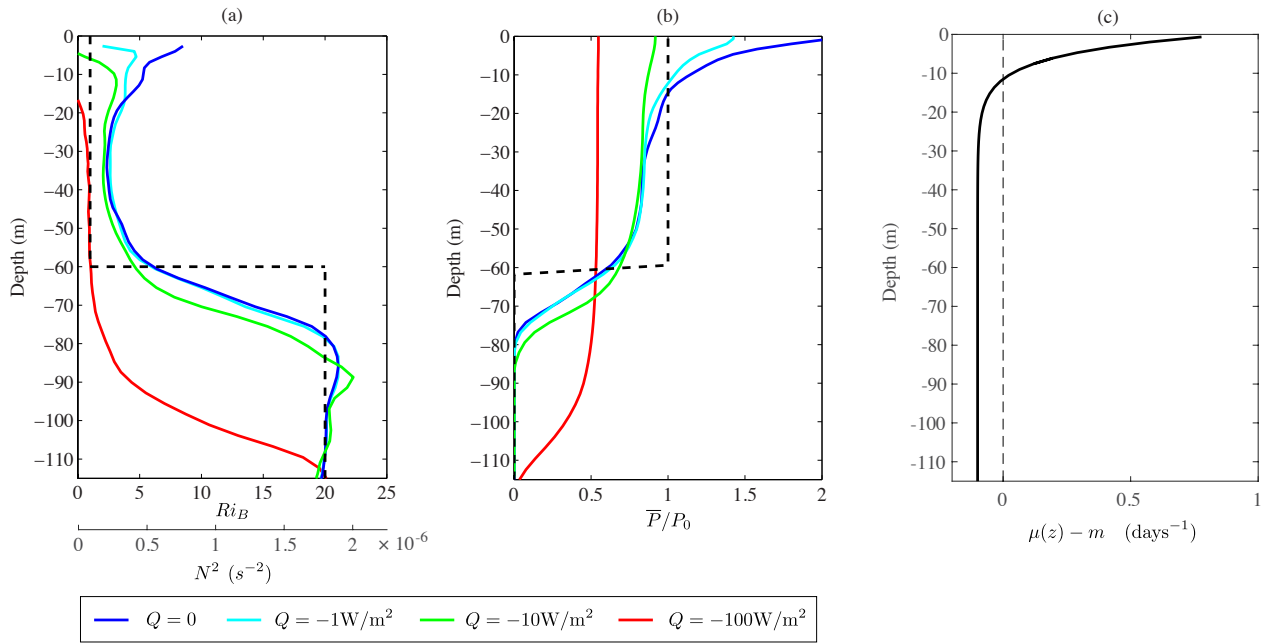


Figure 2. Horizontally averaged profiles of (a) balanced Richardson number, $Ri_B = N^2 f^2 / M^4$ and (b) normalized phytoplankton concentration, \bar{P}/P_0 at $t = 3$ days. Initial profiles are indicated using black dashed lines.

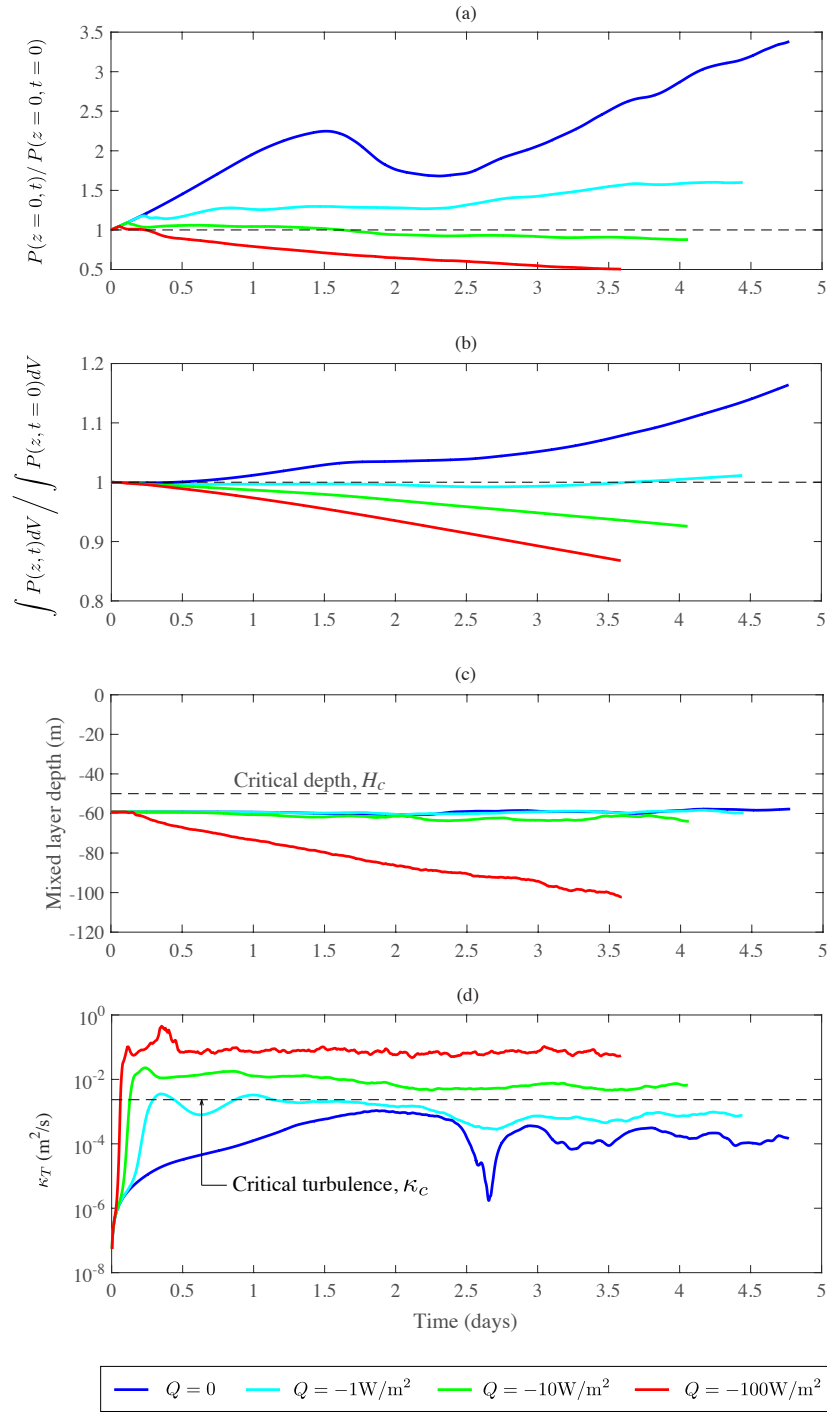


Figure 3. Timeseries of (a) volume integrated phytoplankton concentration and (b) diagnosed turbulent diffusivity, κ_T , defined in Eq. (5). The initial concentration is indicated using a black dashed line in panels (a) and (b).

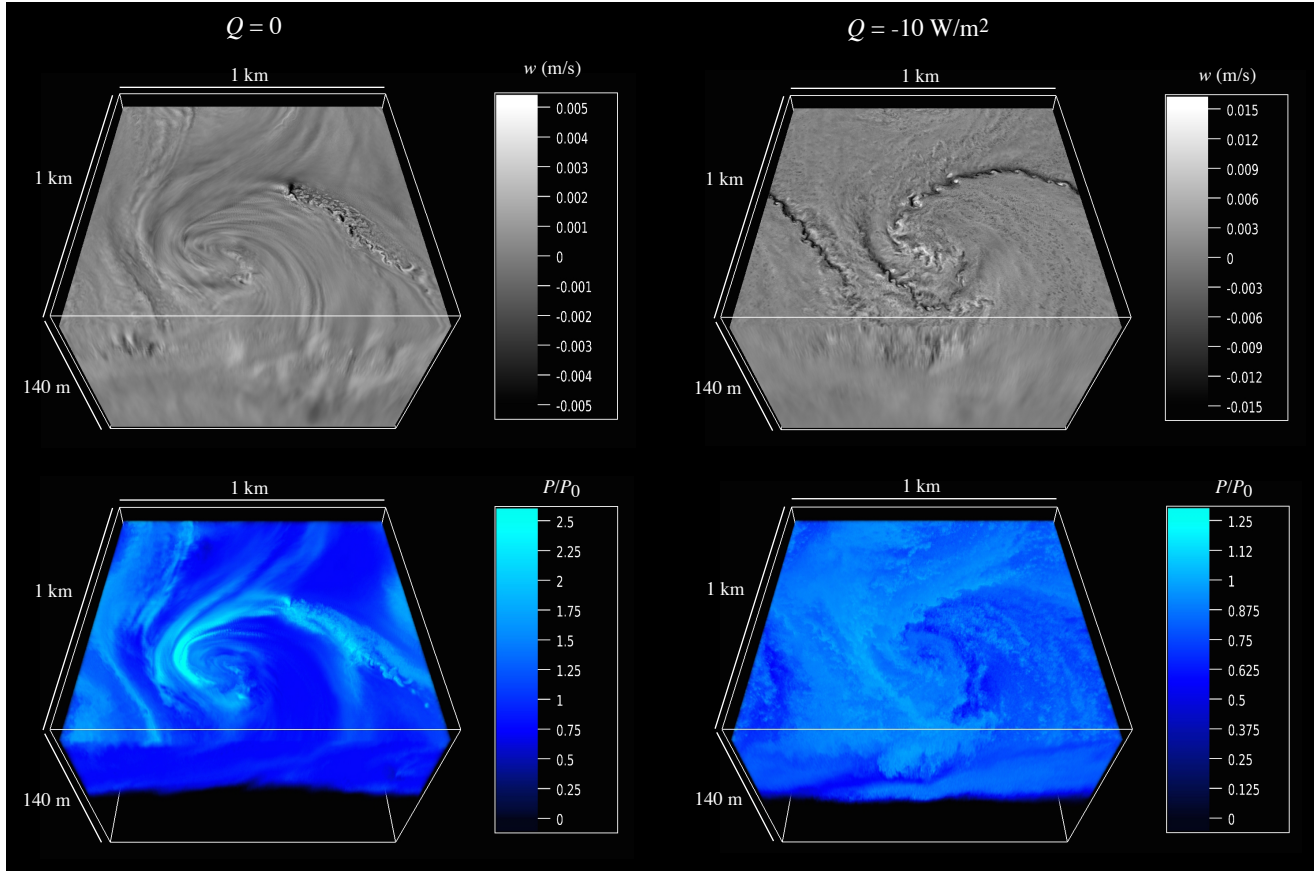


Figure 4. Three-dimensional visualization of vertical velocity (top row) and phytoplankton concentration (bottom row) for the simulations with $Q = 0$ (left column) and $Q = -10 \text{ W/m}^2$ (right column) at $t = 3.5$ days. The upper horizontal slice in each panel is at a depth of 10 m. Note that the color range varies in each panel.

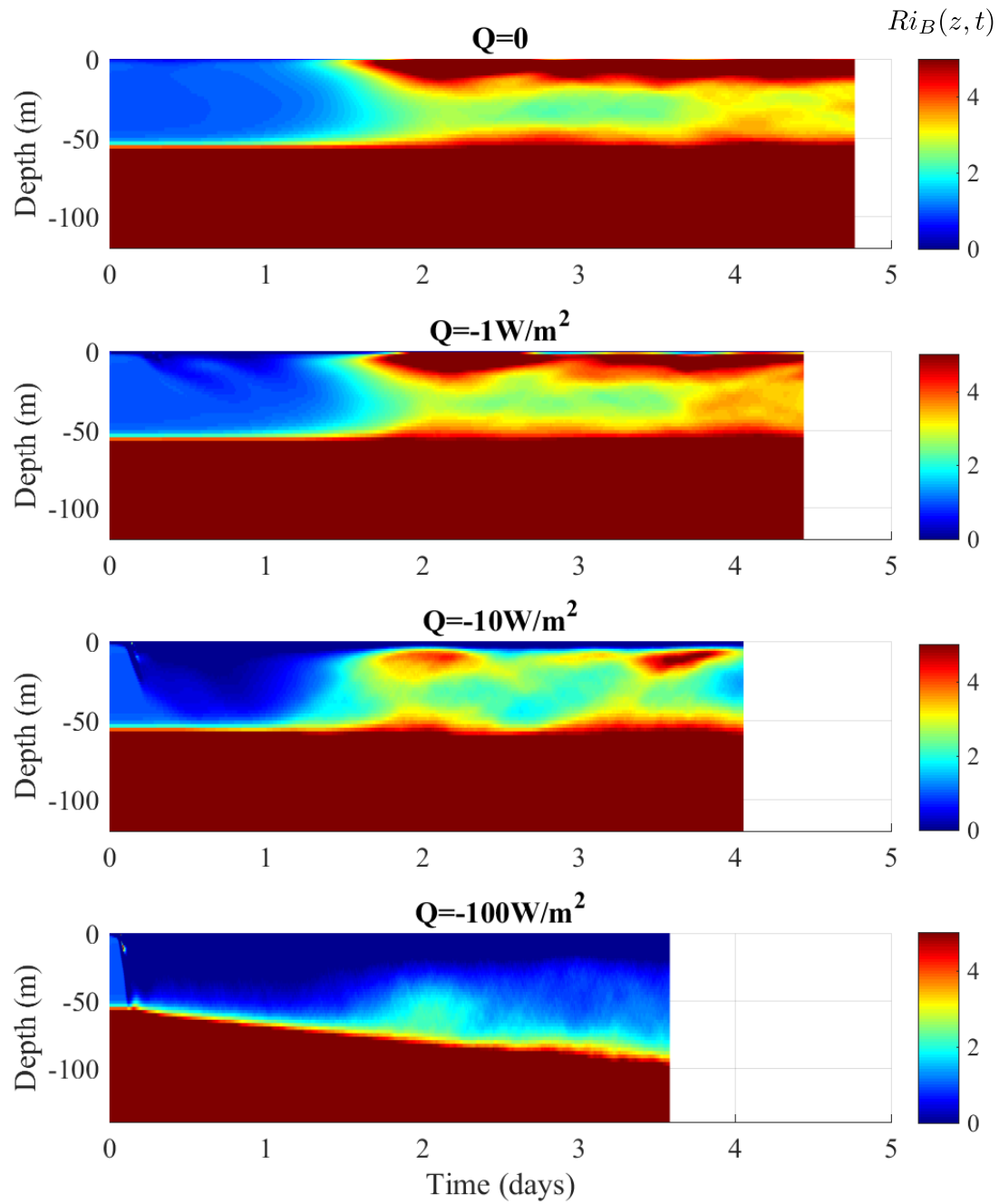


Figure 5. Depth-time plots of the bulk Richardson number for each simulation.

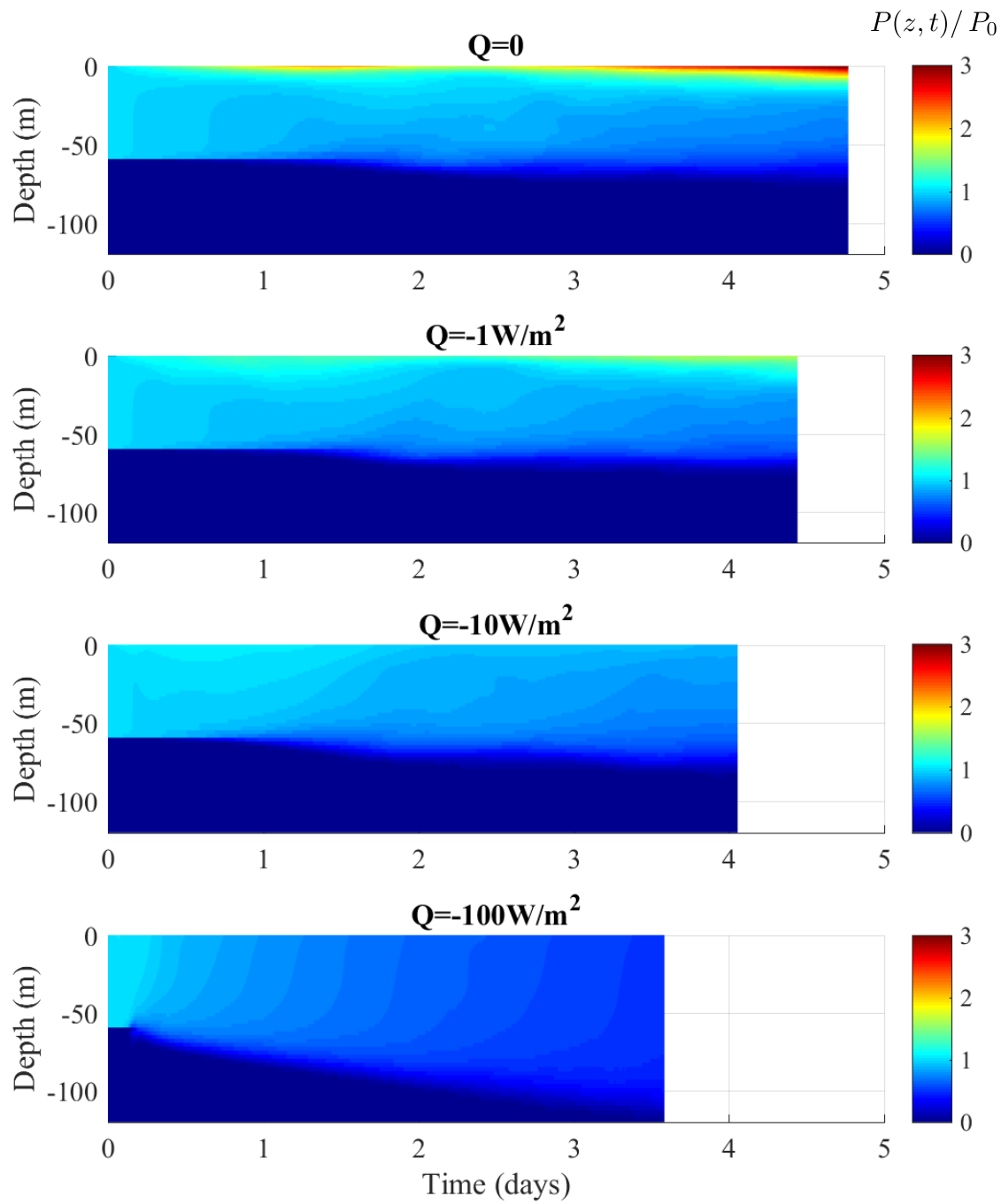


Figure 6. Depth-time plots of the horizontally averaged phytoplankton concentration for each simulation.

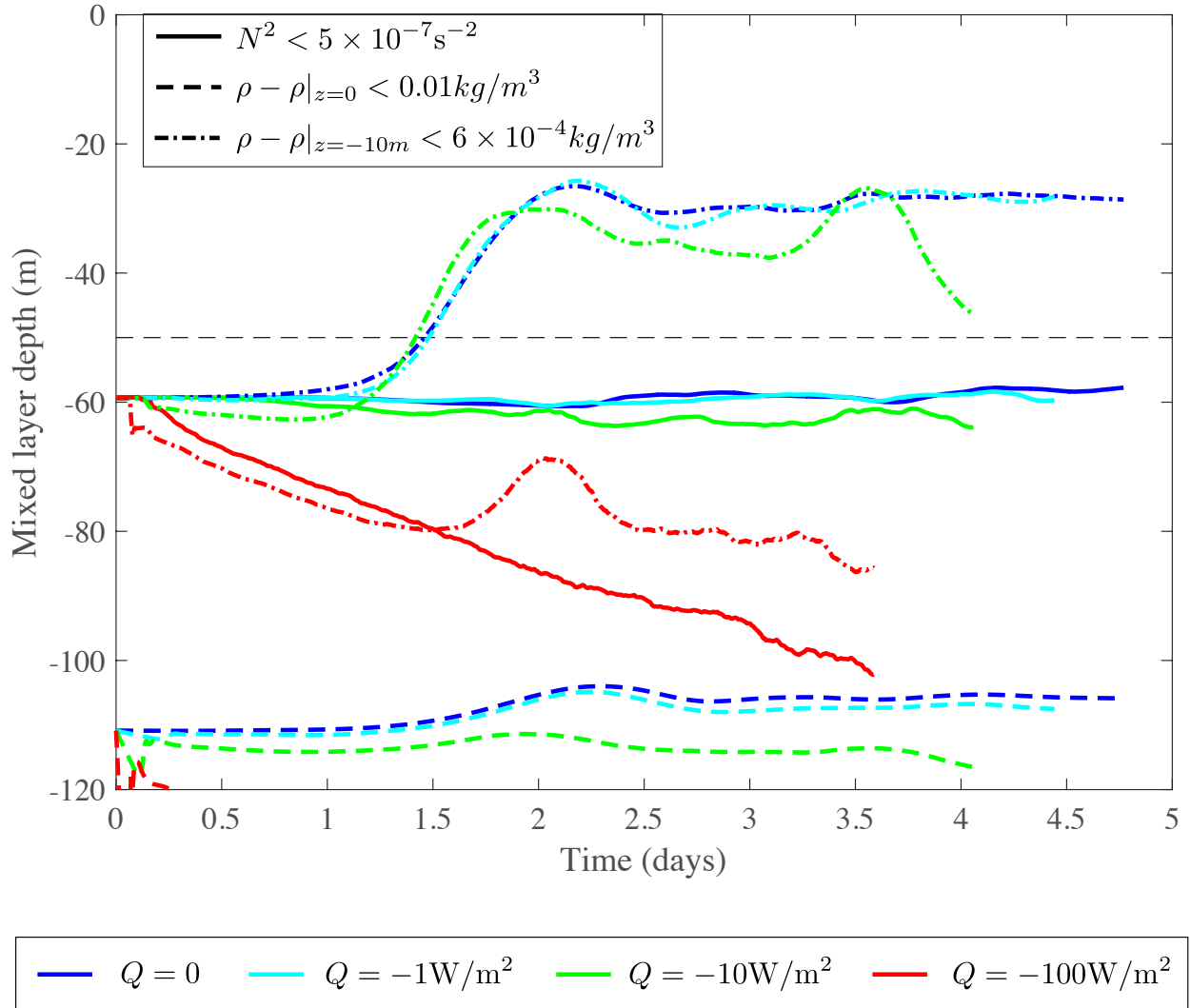


Figure 7. Timeseries of mixed layer depth calculated using three different criteria.

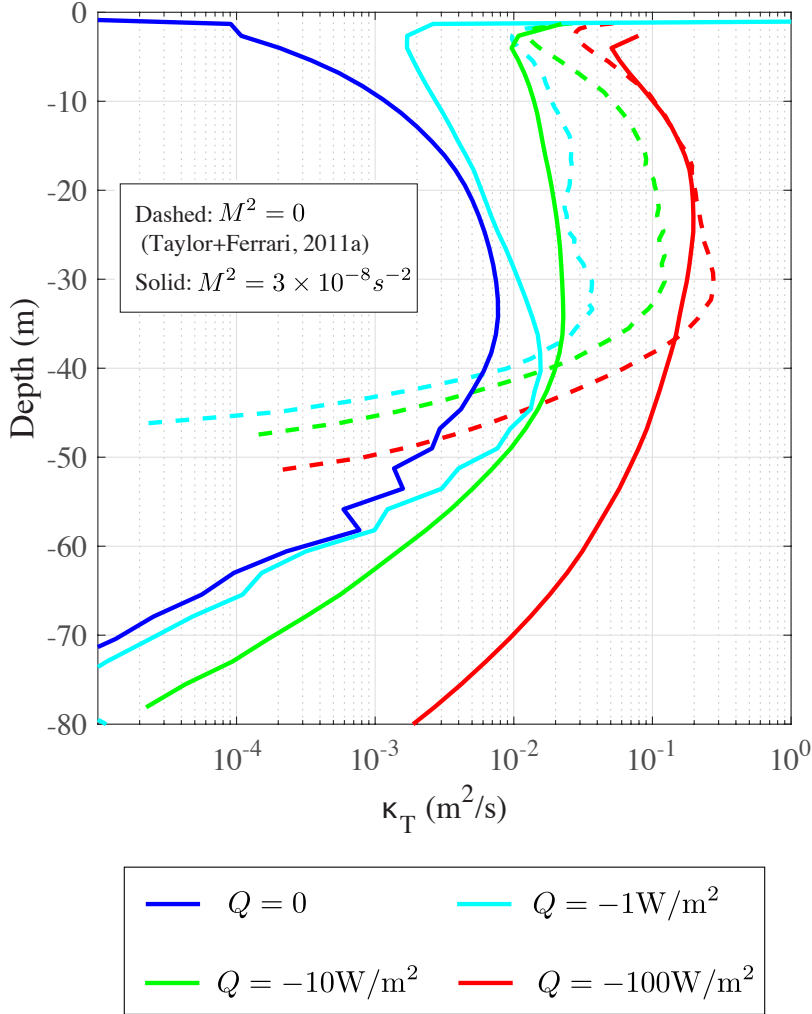


Figure 8. Profiles of the inferred phytoplankton diffusivity. The diffusivity is defined as the ratio of the phytoplankton flux to the vertical phytoplankton derivative, where both are averaged over horizontal planes and in time from 1-1.5 days of model time. The simulations with $M^2 = 3 \times 10^{-8} \text{s}^{-2}$ (solid lines) are the simulations with MLI reported here, the simulations with $M^2 = 0$ (dashed lines) are from *Taylor and Ferrari* [2011a]. Note that in simulations of *Taylor and Ferrari* [2011a], the initial mixed layer depth was 50m, compared to 60m in the simulations reported here. The phytoplankton model and biological parameters are the same in both sets of simulations.

Supporting Information for “Turbulent mixing, restratification, and phytoplankton growth at a submesoscale eddy.”

J. R. Taylor¹

Contents of this file

1. Text S1
2. Figures S1 to S5

Text S1.

1. Numerical method

The numerical simulations use DIABLO, an open-source non-hydrostatic computational fluid dynamics code developed in *Taylor* [2008]. The code solves the incompressible Boussinesq equations using a combination of a pseudo-spectral method to calculate hori-

J.R. Taylor Department of Applied Mathematics and Theoretical Physics University of Cambridge Wilberforce Road CB3 0WA UK (J.R.Taylor@damtp.cam.ac.uk)

¹Department of Applied Mathematics and
Theoretical Physics, University of
Cambridge, Cambridge, UK

zonal derivatives and second-order finite differences to calculate vertical derivatives. The time-stepping algorithm is a mixed implicit/explicit scheme using a 3rd order Runge Kutta method and Crank-Nicolson for viscous/diffusive terms. Further details about the numerical method are available in *Taylor* [2008].

An LES solves a low-pass filtered version of the governing equations. In order to close the equations, a subgrid-scale model is needed to represent the influence of unresolved velocity and density fluctuations on the resolved fields. Here, we have used a modified version of the constant Smagorinsky model proposed by *Kaltenbach et al.* [1994]. This model has been used previously in several previous related studies (e.g. *Taylor and Ferrari* [2010, 2011]; *Thomas et al.* [2013]). For simplicity, the subgrid-scale diffusivity for density and phytoplankton are assumed to match the viscosity (the subgrid-scale Prandtl and Schmidt numbers are set to 1).

The model is run in a so-called ‘frontal zone’ configuration introduced by *Taylor and Ferrari* [2009]. In this configuration, the total buoyancy, b_T , is decomposed into a linear profile plus perturbations:

$$b_T(x, y, z, t) = M^2 x + b'(x, y, z, t). \quad (1)$$

This form is inserted into the governing equations to yield evolution equations for b' . The model then solves these equations with periodic boundary conditions applied to b' . Effectively, this keeps the difference in total buoyancy across the domain constant in space and time. Although this configuration is artificial, it represents intensification of buoyancy gradients due to frontogenesis or differential heating at scales that are too large

to be resolved in the domain. To prevent spurious reflections of internal gravity waves from the bottom of the computational domain, a sponge layer was added from 120-140m. Before starting convective forcing and initializing the phytoplankton model, MLI was allowed to develop from a small-amplitude random perturbation. To reduce the computational cost, this spinup was performed using a coarser resolution with 128 gridpoints in each horizontal direction, but the same vertical grid spacing. During the spinup period, the volume-averaged turbulent kinetic energy increases from $5.5 \times 10^{-12} \text{m}^2/\text{s}^2$ to $3.0 \times 10^{-8} \text{m}^2/\text{s}^2$, and the energy at the end of the spinup was dominated by the most unstable mode with a characteristic horizontal scale of 1km. Spectral interpolation is then used to initialize each of the high resolution simulations. For convenience, $t = 0$ corresponds to the end of the spinup period, when the phytoplankton model is initialized and convective forcing begins.

2. Visualizations

Figure 1 shows 3D visualizations of the vertical velocity and phytoplankton concentration from the simulations with $Q = 0$ and $Q = -10\text{W}/\text{m}^2$ at $t = 3.5$ days (the same time as shown in Figure 1). The vertical velocity is relatively large, exceeding 5 mm/s, in the unforced simulation ($Q = 0$). Large vertical velocity occurs in bands wrapped around the submesoscale eddy and in intermittent bursts. The turbulent bursts are qualitatively similar to those seen in recent studies of stratified turbulence [*Rorai et al.*, 2014, e.g.]. When $Q = -10\text{W}/\text{m}^2$, the vertical velocity is up to three times larger, exceeding 1.5 cm/s. Here, strong downdrafts are visible along lines wrapped around the submesoscale eddy. It seems likely that this strong vertical velocity is associated with submesoscale

frontogenesis [*Shakespeare and Taylor, 2013, e.g.*] driven by strain associated with the submesoscale eddy. Possible indications of horizontal shear instabilities are also visible along this band, notably on the right side of the image.

The corresponding phytoplankton concentration is shown in the bottom row of Figure 1. In the unforced case (Fig. 1 lower left panel) swirls of high phytoplankton concentration are seen wrapping in and around the submesoscale eddy. At a given horizontal level, the phytoplankton concentration varies by more than a factor of 5, indicating the very strong spatial inhomogeneity that develops. In contrast, the phytoplankton concentration is more uniform in the simulation with $Q = -10\text{W/m}^2$ (Fig. 1 lower right panel), and the maximum concentration is significantly lower. Still, physical features of the flow are visible in the phytoplankton concentration including the submesoscale eddy, small-scale convective motions, and banding in the vertical.

3. Time evolution of vertical density and phytoplankton profiles

Figure 2(a) showed profiles of the bulk Richardson number, $Ri_B = \overline{N^2} f^2 / M^4$ at 3.5 days of simulation time. A more complete picture of the mean stratification can be seen using depth-time plots of the balanced Richardson number as shown in Figure 2. Note that here the colorbar is saturated to emphasize the stratification that develops within the mixed layer. In the three cases with the weakest forcing ($Q = 0, -1, \text{ and } -10 \text{ W/m}^2$), the boundary between the strongly stratified thermocline and the mixed layer remains relatively constant, consistent with the mixed layer depth shown in Figure 3(c). These cases all develop stronger stratification near the surface, although the strength of this stratification decreases with increasing forcing.

A non-zero stratification with $Ri_B \simeq 1$ develops in the case with $Q = -100 \text{ W/m}^2$, underlying a region with $N^2 < 0$ and active convection. This is consistent with the dynamics of forced symmetric instability (SI) reported in *Taylor and Ferrari* [2010] where a prediction for the boundary between the convective and SI layers is consistent with the results presented here. An important difference here is that mixed layer eddies have strongly distorted the fronts on which SI might be active. A detailed analysis of the interaction between forced SI and MLI will be left for future work.

A similar depth-time plot of the horizontally-averaged phytoplankton concentration is shown in Figure 3. Large near-surface concentrations quickly develop in the simulations with $Q = 0$ and -1 W/m^2 . The reduction in the surface phytoplankton concentration seen in Figure 3(a) from about 1.5-2 days in the case with $Q = 0$ is accompanied by an increase in the phytoplankton concentration between $-25\text{m} < z < 0$. This is consistent with the interpretation that downward advection of phytoplankton associated with strong frontogenesis is responsible for delaying the phytoplankton bloom in this case.

4. Mixed layer depth

As discussed in the main text, the definition of mixed layer depth is somewhat ambiguous given the significant vertical structure in the upper ocean stratification seen here, particular in the cases with weak convective forcing. In addition to the definition used in the main text, two other examples of the mixed layer depth are shown in Figure 4. For reference, the critical depth, $H_c = 50\text{m}$, is indicated using a thin dashed black line.

The definition used by *Mahadevan et al.* [2012] is the depth where the local potential density changes by 0.01 kg/m^3 from the surface value. This definition is shown using

dashed lines in Figure 4. As noted in the text, the initial stratification in the mixed layer is very weak by traditional measures, with a change of $5.4 \times 10^{-4} kg/m^3$ in the upper 60m at the start of each simulation. Therefore to reach a value of $0.01 kg/m^3$, this definition of the mixed layer must include some of the more strongly stratified thermocline. In fact, the initial mixed layer depth using this criteria is about 110m. The mixed layer, defined in this way, shoals very slightly in the simulations with weak convective forcing, but always remains larger than 100m, and much deeper than the critical depth of $H_c = 50m$.

A more sensitive definition of the mixed layer depth can be constructed using the initial density difference in the upper 60m. The mixed layer depth calculated using this definition is shown as dash-dotted lines in Figure 4. In the LES, a convective layer with $N^2 < 0$ develops near the surface. To avoid this convective layer as much as possible, a threshold of $6 \times 10^{-4} kg/m^3$ is chosen using the difference between the local density and the density at a depth of 10m. With this definition, the restratification in the cases with $Q = 0, -1,$ and $-10 W/m^2$ is sufficient to shoal the mixed layer above the critical depth at about 1.5 days of simulation time, while the mixed layer remains below the critical depth in the simulation with $Q = -100 W/m^2$. Importantly, the mixed layer depth is very similar in the cases with $Q = 0, -1,$ and $-10 W/m^2$ which have very similar density profiles but very different phytoplankton responses. The timeseries of the mixed layer depth and critical depth and the surface and depth-integrated phytoplankton concentration shown in Figures 3(a) and (b), are not consistent with the critical depth hypothesis.

References

- Kaltenbach, H.-J., T. Gerz, and U. Schumann (1994), Large-eddy simulation of homogeneous turbulence and diffusion in stably stratified shear flow, *Journal of Fluid Mechanics*, *280*, 1–40.
- Mahadevan, A., E. D’Asaro, C. Lee, and M. J. Perry (2012), Eddy-driven stratification initiates north atlantic spring phytoplankton blooms, *Science*, *337*(6090), 54–58.
- Rorai, C., P. Mininni, and A. Pouquet (2014), Turbulence comes in bursts in stably stratified flows, *Physical Review E*, *89*(4), 043,002.
- Shakespeare, C. J., and J. Taylor (2013), A generalized mathematical model of geostrophic adjustment and frontogenesis: uniform potential vorticity, *Journal of Fluid Mechanics*, *736*, 366–413.
- Taylor, J. (2008), Numerical simulations of the stratified oceanic bottom boundary layer, Ph.D. thesis, University of California, San Diego.
- Taylor, J., and R. Ferrari (2010), Buoyancy and wind-driven convection at a mixed-layer density fronts, *Journal Physical Oceanography*, *40*, 1222–1242.
- Taylor, J. R., and R. Ferrari (2009), On the equilibration of a symmetrically unstable front via a secondary shear instability, *Journal of Fluid Mechanics*, *622*, 103–113.
- Taylor, J. R., and R. Ferrari (2011), Shutdown of turbulent convection as a new criterion for the onset of spring phytoplankton blooms, *Limnology and Oceanography*, *56*(6), 2293–2307.
- Thomas, L. N., J. R. Taylor, R. Ferrari, and T. M. Joyce (2013), Symmetric instability in the gulf stream, *Deep Sea Research Part II: Topical Studies in Oceanography*, *91*,

96–110.

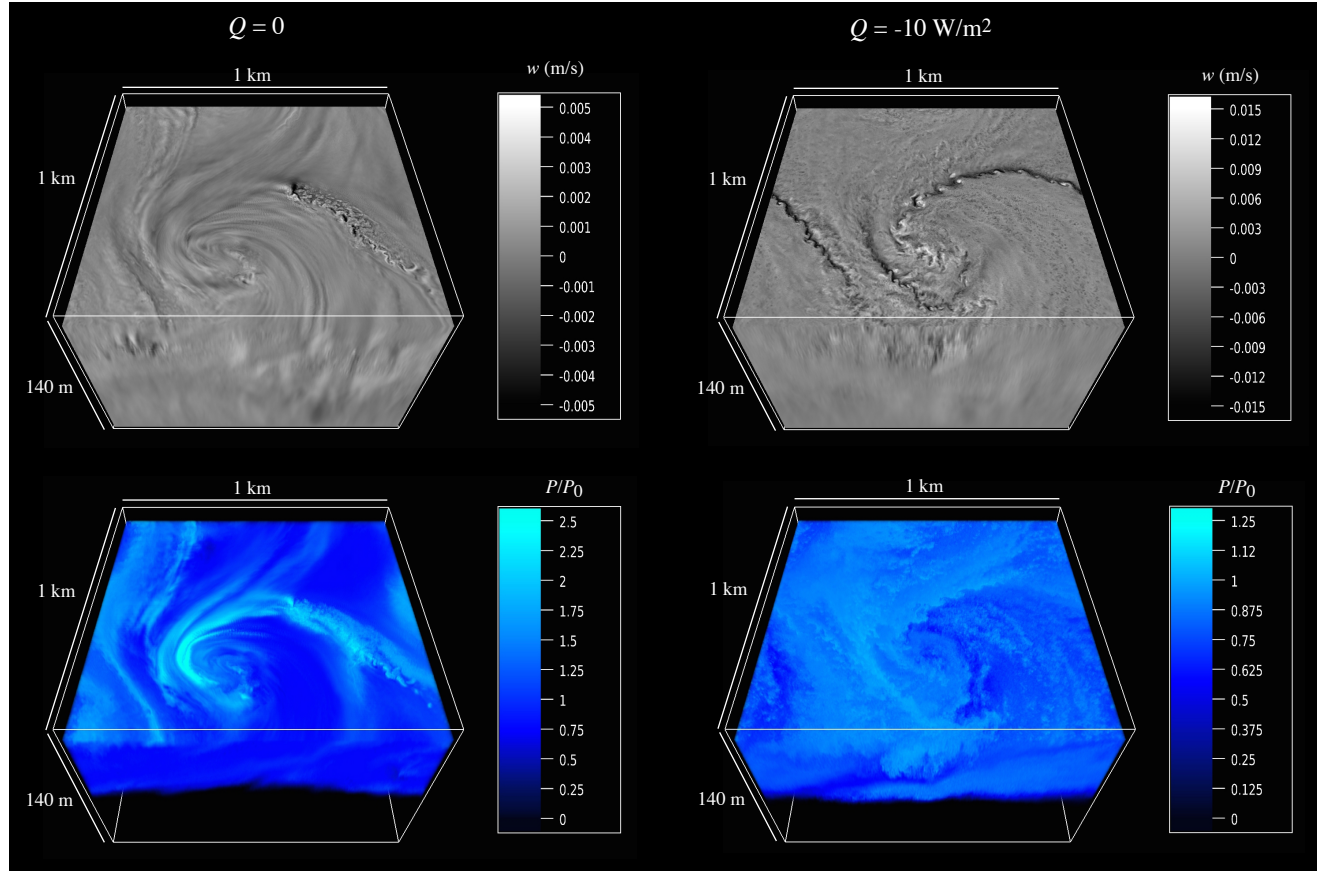


Figure 1. Three-dimensional visualization of vertical velocity (top row) and phytoplankton concentration (bottom row) for the simulations with $Q = 0$ (left column) and $Q = -10 \text{ W/m}^2$ (right column) at $t = 3.5$ days. The upper horizontal slice in each panel is at a depth of 10m. Note that the color range varies in each panel.

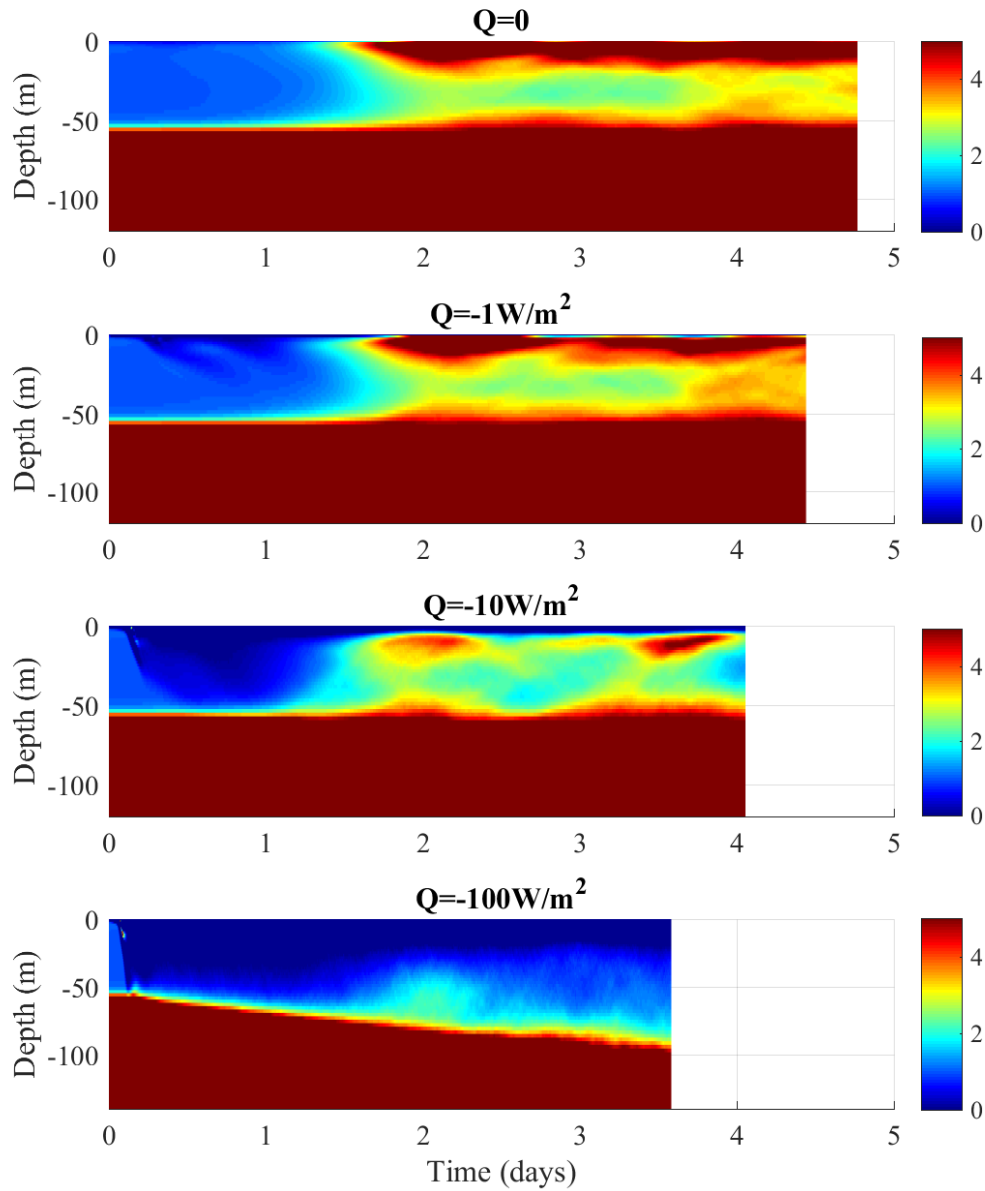


Figure 2. Depth-time plots of the bulk Richardson number for each simulation.

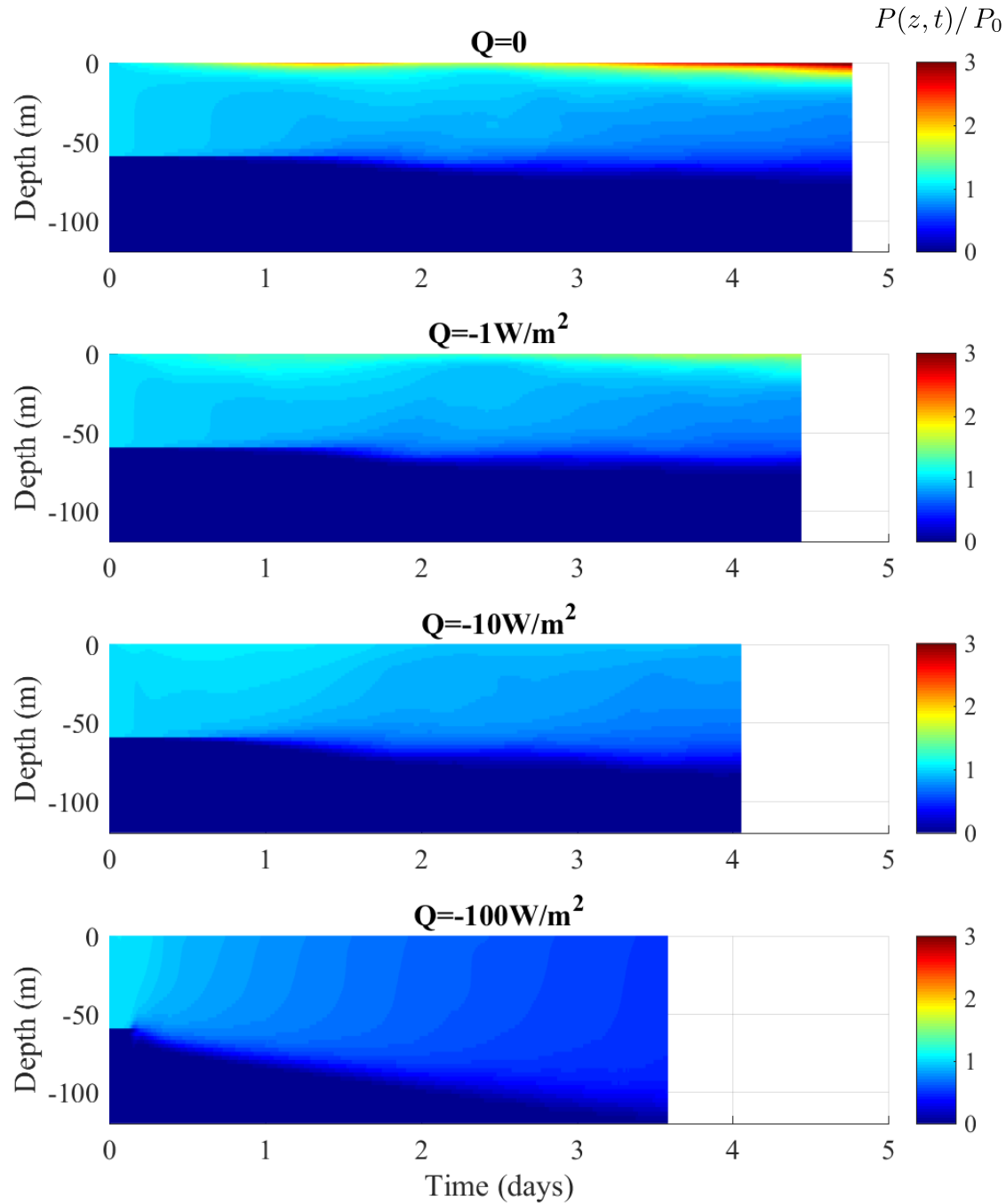


Figure 3. Depth-time plots of the horizontally averaged phytoplankton concentration for each simulation.

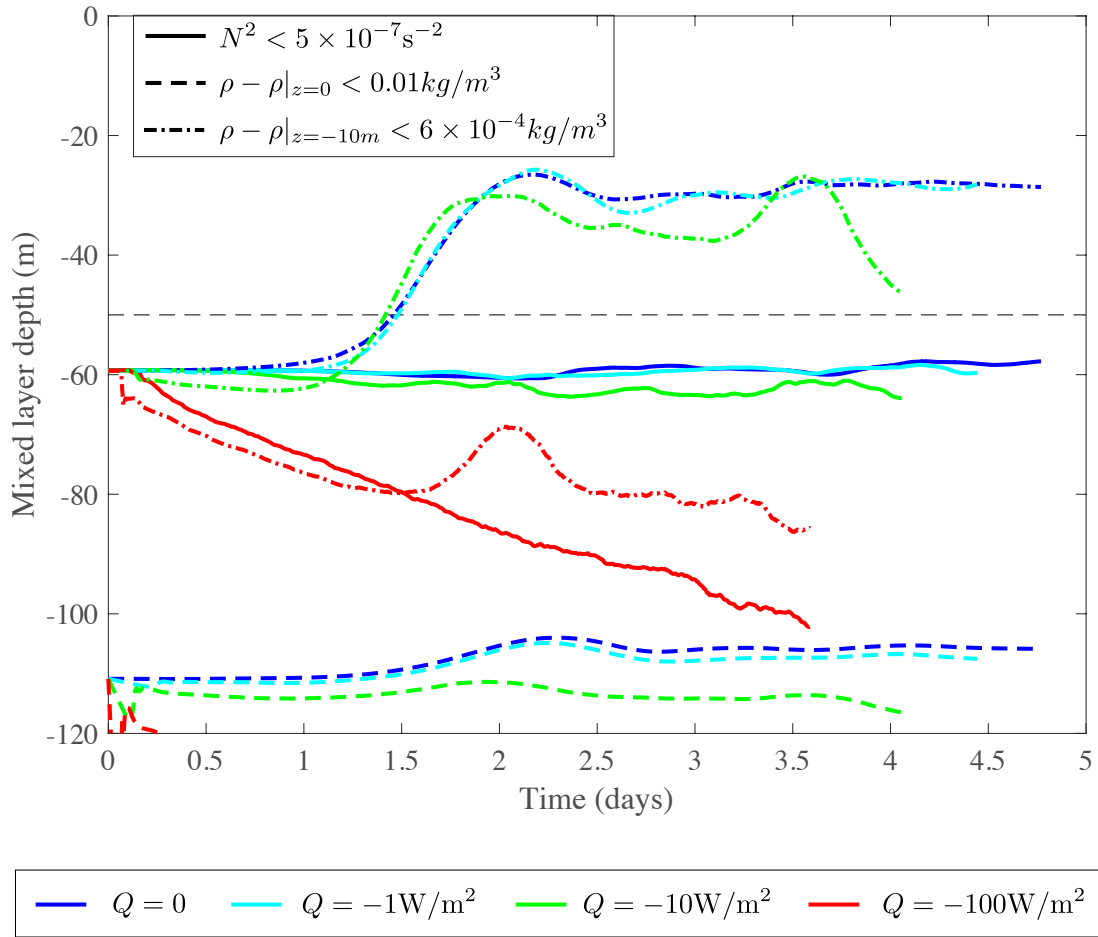


Figure 4. Timeseries of mixed layer depth calculated using three different criteria.

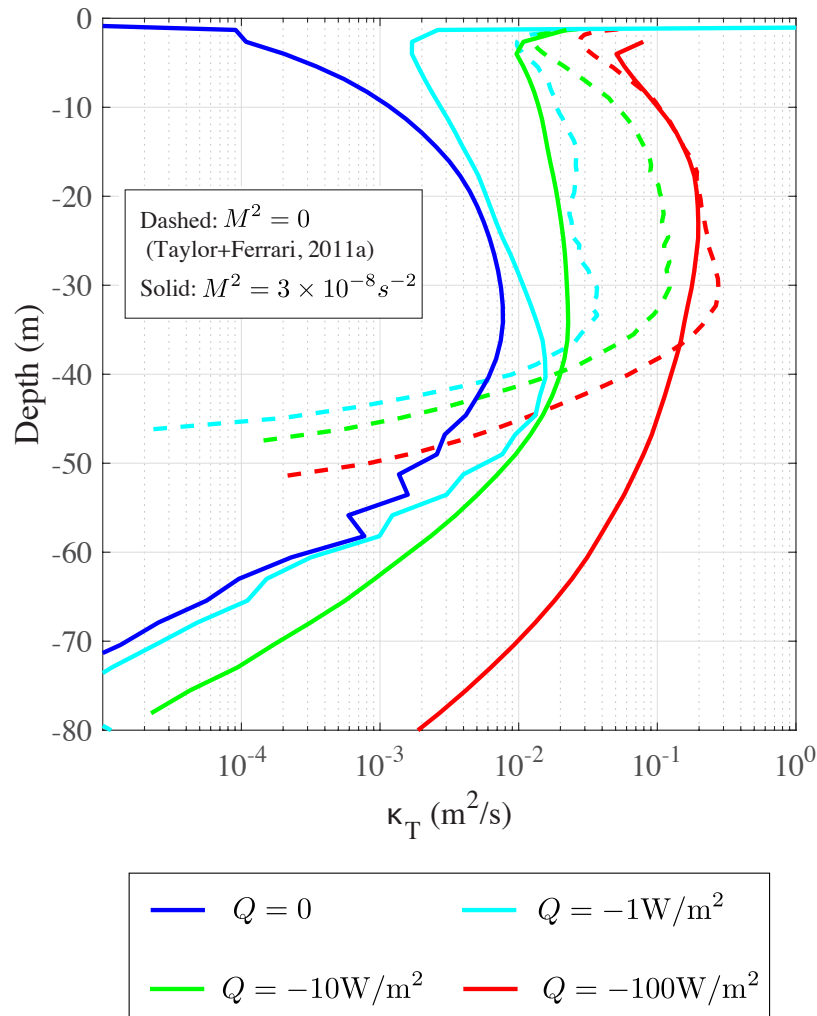


Figure 5. Profiles of the inferred phytoplankton diffusivity. The diffusivity is defined as the ratio of the phytoplankton flux to the vertical phytoplankton derivative, where both are averaged over horizontal planes and in time from 1-1.5 days of model time. The simulations with $M^2 = 3 \times 10^{-8} \text{s}^{-2}$ (solid lines) are the simulations with MLI reported here, the simulations with $M^2 = 0$ (dashed lines) are from *Taylor and Ferrari* [2011]. Note that in simulations of *Taylor and Ferrari* [2011], the initial mixed layer depth was 50m, compared to 60m in the simulations reported here. The phytoplankton model and biological parameters are the same in both sets of simulations.